

Non-locally sensing the spin states of individual atomic-scale nanomagnets

Shichao Yan^{1,2,†,*}, Luigi Malavolti^{1,2}, Jacob A. J. Burgess^{1,2}, Sebastian Loth^{1,2,*}

¹ *Max Planck Institute for the Structure and Dynamics of Matter, 22761 Hamburg, Germany*

² *Max Planck Institute for Solid State Research, 70569 Stuttgart, Germany*

[†] *present address: Department of Physics, University of Illinois at Urbana-Champaign, IL 61801 USA*

**email: sebastian.loth@mpsd.mpg.de, yansc@illinois.edu*

Quantum spin systems can provide unprecedented accuracy and sensitivity compared to classically-based sensors. Here we used a quantum spin sensor consisting of three Fe atoms on a monolayer copper nitride surface to probe the magnetic states of nearby nanomagnets. We detect minute magnetic interactions by measuring variations in the spin relaxation time of the spin sensor. The distance between the nanomagnets and the sensor can be changed discretely by atom manipulation using a low-temperature scanning tunneling microscope. We can sense nanomagnets as far away as 3 nanometers, that couple to the sensor with interaction strengths as low as 6 micro-electron volts. By making use of weak inter-atomic exchange interaction the Fe-atom-based sensor can detect nanomagnets possessing no net spin. This scheme permits simultaneously sensing the magnetic states of multiple nanomagnets with a single quantum spin sensor.

Sensing individual magnetic nano-objects continues to present a challenge in physical and biological sciences (1, 2). A sensor able to detect the magnetic state of individual nanomagnets will enable powerful applications ranging from readout of the magnetic memory to the detection of spins in complex biological molecules (2, 3). Properties of quantum spin systems, such as magnetic stability (4) and spin coherence (5-7), depend sensitively on the local conditions of the spin system. Therefore, they can be used to great effect as sensors for magnetic environments. For example, the environmental dependence of nuclear spin relaxation times of water protons in tissues is the fundamental basis of magnetic resonance imaging (8, 9). Great effort is directed toward increasing the spatial resolution and sensitivity of spin detection with a variety of techniques using quantum systems, such as spin to charge conversion in quantum dots (10), magnetic resonance force microscopy (1, 11) and nitrogen-vacancy (NV) centers in diamond which have achieved nanometer resolution (2, 3, 12).

For efficient detection of atomic-scale magnetic objects, such as individual spins or their local magnetic fields, it is desirable to have an atomic-scale sensor which can be placed in close proximity. Magnetic atoms on surfaces are prototypical quantum spin systems (13) and can be positioned at will by atom manipulation with scanning probe tips (14, 15). Their magnetic properties are sensitive to

the local atomic environments and scanning tunneling microscopy (STM) measures the influence of local conditions by detecting, for example, the Kondo effect (16, 17), magnetic anisotropy (13, 18, 19) and spin dynamics (20, 21) of individual atoms.

Here we show that the spin dynamics of a few-atom quantum spin system can be used to non-locally sense the magnetic state of a nearby nanomagnet. We use a low-temperature scanning tunneling microscope to assemble the quantum spin sensor and the target nanomagnets with Fe atoms on a monolayer copper nitride surface on a Cu(100) substrate (13, 17). The spin sensor is assembled as a linear atomic chain consisting of three Fe atoms, Fe_3 (13, 22). Subsequently, a nanomagnet exhibiting two stable magnetic states is built nearby as part of the spin environment of Fe_3 , Fig. 1A. We then measure the spin relaxation time (T_1) of the spin sensor, Fe_3 , by electronic pump-probe spectroscopy (20, 22).

The nanomagnet is constructed with an even number of antiferromagnetically coupled atoms. It has no net spin and switches spontaneously between two Néel states, Fig. 1B (14), signified by alternating apparent height of the constituent Fe atoms in spin-polarized STM topographs. The Fe_3 spin sensor has a unique spin ground state and an excited state (the first excited state) with a sub-microsecond spin relaxation time, T_1 . We find that Fe_3 switches between two different spin relaxation times concomitant with the nanomagnet switching between its two Néel states: Figure 1B shows that the spin relaxation curves differ in amplitude at finite pump-probe delay time. Hence, recording the electronic pump-probe signal at fixed pump-probe delay over time yields a trace of the two-state switching of the nearby nanomagnet, Fig. 1C. Increasing the delay time from 150 ns to 250 ns reduces the amplitude of the two-state signal until it vanishes when the quantum spin is fully relaxed at 500 ns delay. This confirms the two-state switching in the pump-probe signal is due to the changes in T_1 of the Fe_3 , and substantiates our method of non-locally sensing the magnetic state (Fig. 1C).

While measuring the Fe_3 , the switching rate of the nearby nanomagnet is enhanced compared to its intrinsic switching rate (14). Indeed, by decreasing the amplitude of the pump pulse, the stability of the nanomagnet increases and the switching rate approaches once per tens of minutes for pump pulses of -10 mV amplitude, Fig. 2D. This indicates that the non-local spin sensing method is invasive but it can be made sufficiently weak to allow measurements non-perturbative on the time-scale of minutes (Fig. 1B). This observation is consistent with switching induced by hot carriers that are injected into the sample during the pump pulses and propagate to the nanomagnet (23, 24). At the same time hot carrier injection explains our ability to intentionally switch the nanomagnet even with the tip at several nanometers distance.

The difference in T_1 (ΔT_1) of Fe_3 induced by the Néel-state switching of the nearby nanomagnet can be increased by positioning Fe_3 closer. As shown in Fig. 2A, we gradually decrease the separation between Fe_3 and nanomagnet, and monitor the concomitant changes in the spin relaxation signal. Fe_3 always has longer T_1 when the nearby Fe nanomagnet is in the Néel-state “0” than in state “1”. ΔT_1 becomes larger as the separation between the nanomagnet and Fe_3 decreases (Fig. 2B): at 3.0 nm separation ΔT_1 is 29 ns and increases to 466 ns at 1.1 nm separation.

All measurements investigating the Fe₃-nanomagnet separation were performed with the same nanomagnet on the same copper nitride patch, simply moving the Fe₃ to different locations by STM atom manipulation (Fig. 2A). Still, subtle variations in the dynamical characteristics of Fe₃ in each location are possible due to changes in interaction with the copper nitride substrate (17). Therefore, we calibrate the Fe₃ sensor in each location with a known and spatially uniform interaction: the external magnetic field, Fig. 2C. We find that, for each Néel state of the nanomagnet, the measured T_1 of the Fe₃ sensor scales linearly with external magnetic field for every separation shown in Fig. 2A. The ΔT_1 induced by the switching between two Néel states stays constant with field (Fig. 2C).

Under external magnetic field, the spin ground state of Fe₃ is dominated by $|+2 -2 +2\rangle$ and the first excited state is mostly $|-2 +2 -2\rangle$ (± 2 denotes the expectation value of each atom's spin along the easy magnetic axis). In this regime T_1 of Fe₃ scales linearly with the energy difference between these two states (22):

$$T_1 = \alpha (E_e - E_g) \quad (1)$$

Where E_e and E_g are the energy levels of the first excited and the ground states. The linear dependence of T_1 with magnetic field (Fig. 2C) shows that the energy level splitting scales with the Zeeman energy. Hence the linear coefficient α can be determined by the external magnetic field dependence (Fig. 2C). Typical changes in T_1 are several hundred nanoseconds per tesla (ranging from 450 ns / T to 830 ns / T, Fig. S2). The spin magnitude of the low-energy states of Fe₃ is 2 with the g-factor being close to 2 as well (13, 22). Hence, the Zeeman splitting is 464 $\mu\text{eV} / \text{T}$ (25), so the linear coefficient α in Eq. (1) ranges between 1 to 2 ns / μeV .

Having calibrated α with external magnetic field we can now quantify the magnetic interaction between nanomagnet and Fe₃ spin sensor. T_1 of the Fe₃ varies as the nanomagnet switches from one Néel state to the other and the Néel-state switching is the only change in the local environment. Therefore, the variation in T_1 of the Fe₃ must be induced by the magnetic interaction with the nanomagnet. As the nanomagnet is in Néel-state “0” (Fig. 1B) the magnetic interaction with Fe₃ will decrease the energy of the ground state of the Fe₃ by the interaction energy ΔE . The energy of the first excited state will increase by ΔE because its spin is reversed compared to the ground state (Fig. 3A inset). When the nanomagnet is in Néel-state “1” (Fig. 1B), the energy of the ground state of Fe₃ will be increased and that of the first excited state decreased (Fig. 3A inset). As a consequence, the change in spin relaxation time, ΔT_1 , caused by Néel-state switching of the nanomagnet is:

$$\Delta T_1 = \alpha \cdot 4 \Delta E \quad (2)$$

Where α is the linear coefficient determined in Eq. (1). Fig. 3A shows the magnetic interaction strength ΔE as a function of the separation between the Fe₃ and nanomagnet for the arrangements shown in Fig. 2A. As can be seen, ΔE increases quickly from 6 μeV to 112 μeV as the separation decreases from 3.0 nm to 1.1 nm.

We find the measured magnetic interaction between Fe_3 and the nanomagnet is consistent with a long-range antiferromagnetic exchange interaction between their magnetic atoms. The distance dependence of the exchange energy shown in Fig. 3A is well-described by an isotropic exponential decay with a single decay constant of 0.8 nm (blue line in Fig. 3A) (26), but within the accuracy of our measurement a power-law decay cannot be excluded. The calculated dipolar magnetic interaction, however, can only account for $\sim 5\%$ of the measured interaction energy (black line in Fig. 3A). Long-range super-exchange interaction mediated by the Cu_2N molecular network can also be excluded because magnetic interaction with similar strength ($6 \pm 1 \mu\text{eV}$) can be detected when the Fe_3 and the nanomagnet are built on different Cu_2N patches where the Cu_2N network is broken in between the nanostructures (Fig. 3B).

We note that the sensitivity of the non-local spin sensing measurement is related to the weakest ΔT_1 that can be detected above the noise of the pump probe measurement. This signal-to-noise ratio can be optimized by reducing T_1 of Fe_3 and increasing the repetition rate of the pump probe experiment so that it effectively scales as $\Delta T_1 / T_1$ (Fig. S1) (22). For measurements with a fixed integration time of one minute we found that the Néel-state switching could clearly be detected for the ratio $\Delta T_1 / T_1 > 0.1$ (fig. S1 and S2) with a minimum T_1 of order 10 ns set by the time resolution of our electronic setup. This means that the weakest detectable magnetic interaction in this experiment is $0.6 \mu\text{eV}$ corresponding to sensor-to-nanomagnet distances well above 3.0 nm. The sensitivity could be improved further by higher time resolution of the pump-probe measurement or choosing a quantum spin sensor with higher sensitivity to local magnetic perturbations, i.e., larger α .

This high sensitivity and the non-local nature of spin sensing using a quantum spin allow us to simultaneously identify the state of several nanomagnets in the vicinity of the sensor. Figure 4a shows an area where two Fe nanomagnets were assembled around an Fe_3 . By monitoring the pump-probe signal on Fe_3 with fixed delay time, we can clearly detect four-state switching (Fig. 4B). This corresponds to the four different configurations of the spin environment (labeled (0, 0), (0, 1), (1, 0) and (1, 1) in Fig. 4A). The one-to-one relationship between the four states in the pump-probe signal and the four spin configurations is confirmed by switching to STM imaging mode and acquiring an image after observing the pump-probe signal switching into each state.

The strong signal jump in Fig. 4B is induced by the switching of the right Fe nanomagnet because it is closer to Fe_3 and interacts more strongly. The weak signal jumps are induced by the switching of the left nanomagnet. We can also see the left nanomagnet is less stable than the right nanomagnet as the weak signal jumps happen more frequently (Fig. 4B). This demonstrates that non-local spin sensing with atomic spins can provide detailed information about the magnetic properties of several distant nano-objects.

Our non-local sensing scheme does not require the coherent control of the quantum sensor and can be implemented to detect ferromagnetic nanomagnets (27, 28) and single-molecule magnets (29). Furthermore, it can also be used to non-locally detect other kinds of atomic local conditions on surfaces, such as atomic defects (30), weak magnetic fields (2) and surface strain (31). Finally, we note that atomic spin sensors assembled of magnetic atoms on surfaces may enable a wide range of applications from measurements of spin-spin correlation between nano-objects to fundamental tests of quantum mechanics (32).

References:

1. D. Rugar, R. Budakian, H. J. Mamin, B. W. Chui *Nature* **430**, 329 (2004).
2. J. R. Maze *et al.*, *Nature* **455**, 644 (2008).
3. G. Balasubramanian *et al.*, *Nature* **455**, 648 (2008).
4. I. G. Rau *et al.*, *Science* **344**, 988 (2014).
5. J. Du *et al.*, *Nature* **461**, 1265 (2009).
6. L. Childress *et al.*, *Science* **314**, 281 (2006).
7. G. de Lange, Z. H. Wang, D. Ristè, V. V. Dobrovitski, R. Hanson *Science* **330**, 60 (2010).
8. I. L. Pykett *et al.*, *Radiology* **143**, 157 (1982).
9. R. Damadian *Science* **171**, 1151 (1971).
10. J. M. Elzerman *et al.*, *Nature* **430**, 431 (2004).
11. C. L. Degen, M. Poggio, H. J. Mamin, C. T. Rettner, D. Rugar *Proc. Natl. Acad. Sci. U. S. A.* **106**, 1313 (2009).
12. H. J. Mamin *et al.*, *Science* **339**, 557 (2013).
13. C. F. Hirjibehedin *et al.*, *Science* **317**, 1199 (2007).
14. S. Loth, S. Baumann, C. P. Lutz, D. M. Eigler, A. J. Heinrich *Science* **335**, 196 (2012).
15. D. M. Eigler, E. K. Schweizer *Nature* **344**, 524 (1990).
16. V. Madhavan, W. Chen, T. Jamneala, M. F. Crommie, N. S. Wingreen *Science* **280**, 567 (1998).
17. J. C. Oberg *et al.*, *Nat. Nano.* **9**, 64 (2014).
18. A. F. Otte *et al.*, *Nat. Phys.* **4**, 847 (2008).
19. S. Yan, D.-J. Choi, J. A. J. Burgess, S. Rolf-Pissarczyk, S. Loth *Nano Lett.* **15**, 1938 (2015).
20. S. Loth, M. Etzkorn, C. P. Lutz, D. M. Eigler, A. J. Heinrich *Science* **329**, 1628 (2010).
21. B. W. Heinrich, L. Braun, J. I. Pascual, K. J. Franke *Nat. Phys.* **9**, 765 (2013).
22. S. Yan, D.-J. Choi, J. A. J. Burgess, S. Rolf-Pissarczyk, S. Loth *Nat. Nano.* **10**, 40 (2015).
23. J. N. Ladhent *et al.*, *ACS Nano* **9**, 7287 (2015).
24. P. Maksymovych, D. B. Dougherty, X.-Y. Zhu, J. T. Yates *Phys. Rev. Lett.* **99**, 016101 (2007).
25. See Supporting Materials.
26. E. Simon, B. Újfalussy, B. Lazarovits, A. Szilva, L. Szunyogh, G. M. Stocks *Phys. Rev. B* **83**, 224416 (2011).
27. A. A. Khajetoorians *et al.*, *Science* **339**, 55 (2013).
28. A. Spinelli, B. Bryant, F. Delgado, J. Fernández-Rossier, A. F. Otte *Nat. Mater.* **13**, 782 (2014).
29. M. Mannini, *et al.*, *Nat. Mater.* **8**, 194 (2009).
30. J. Repp, G. Meyer, S. Paavilainen, F. E. Olsson, M. Persson *Phys. Rev. Lett.* **95**, 225503 (2005).
31. N. Levy *et al.*, *Science* **329**, 544 (2010).
32. S. Popescu *Nat. Phys.* **10**, 264 (2014).

Acknowledgments:

We thank A. Rubio and E. Simon for fruitful discussions and E. Weckert and H. Dosch, (Deutsches Elektronen-Synchrotron, Germany) for providing lab space. J.A.J.B. acknowledges postdoctoral fellowships from the Alexander von Humboldt foundation and the Natural Sciences and Engineering Research Council of Canada.

Figure 1:

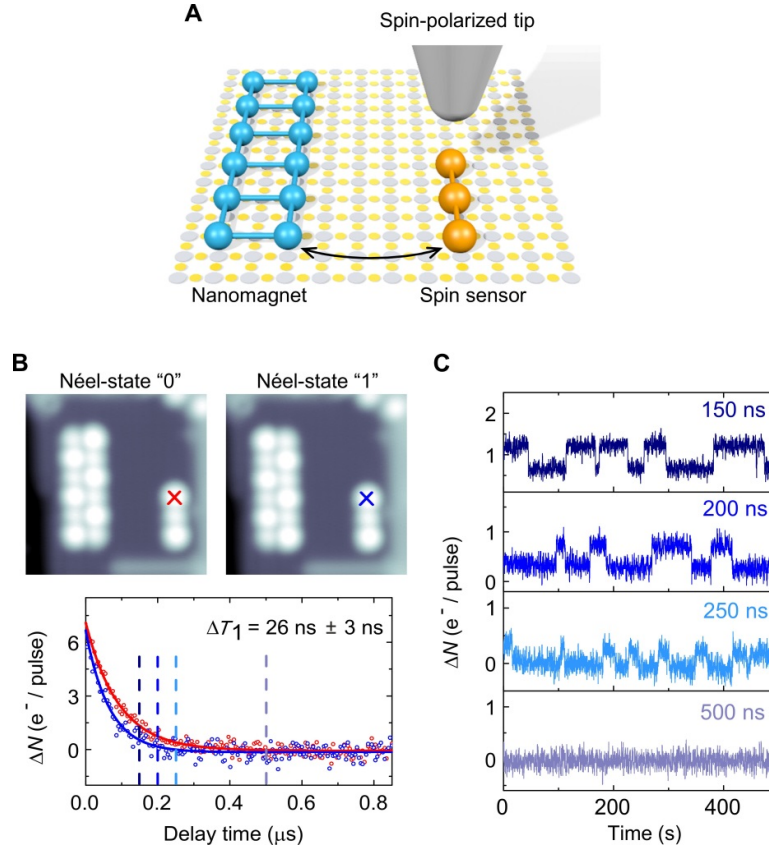


Fig. 1. Non-local sensing scheme. (A) Schematic of the experimental setup. A quantum spin sensor (orange) and a nanomagnet (blue) are assembled from individual Fe atoms on a Cu₂N/Cu(100) surface (Cu: yellow circles; N: grey circles) and interact weakly with each other. The spin-polarized probe tip of a STM (grey) measures the spin relaxation time of the spin sensor. (B) Top panel: spin-polarized STM topographs of the Fe₃ spin sensor and an Fe nanomagnet. The nanomagnet switches between two Néel states. The distance between Fe₃ and nanomagnet is 3.0 nm. Image size (6.6×6.6) nm², color from low (black) to high (white), tunnel junction setpoint, 5 mV, 50 pA. Bottom panel: pump-probe spectra of Fe₃ (red and blue dots) recorded at the position marked in the topographs as the nanomagnet stays in Néel-state "0" or Néel-state "1". Solid lines are exponential decay fits to the experimental data showing that the spin relaxation time of Fe₃ differs by ΔT_1 between both curves. (C) Time traces of the pump-probe signal measured on Fe₃ showing the two-state switching of the distant nanomagnet. The signal amplitude diminishes with increasing delay time between the pump and probe pulses (chosen delay times are indicated by vertical lines in B).

Figure 2:

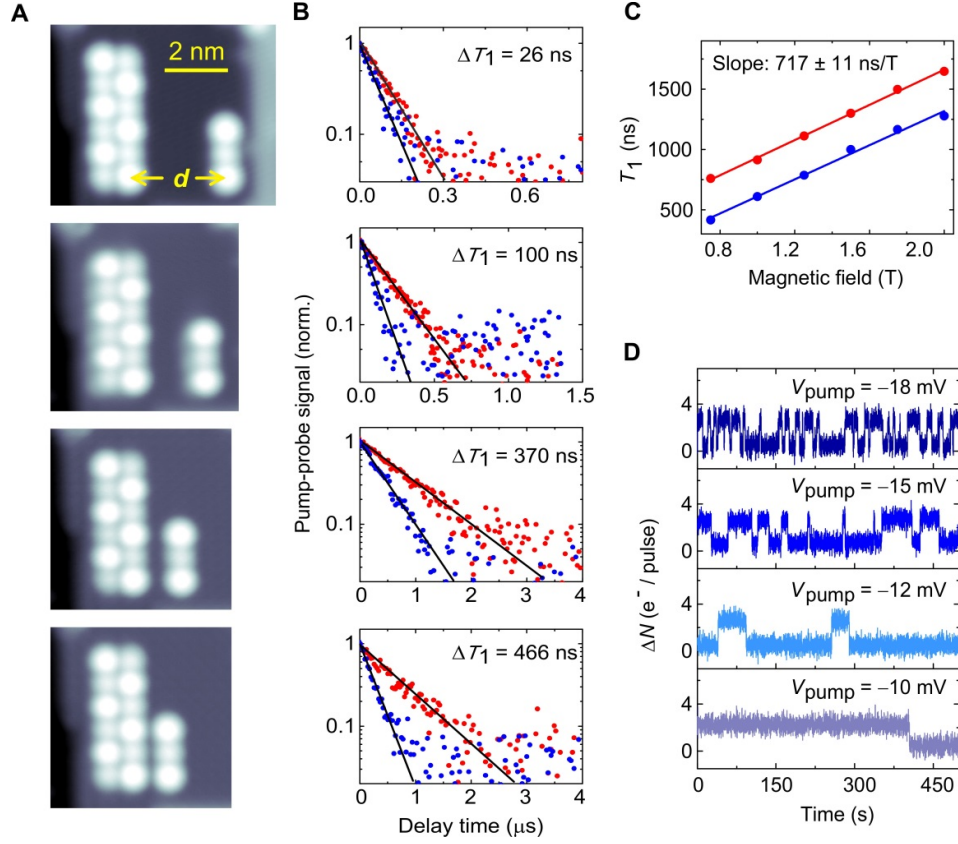


Fig. 2. Distance, magnetic-field and pump-voltage dependence of non-local spin sensing. (A) Spin-polarized STM topographs of different separations, d , between Fe_3 and nanomagnet. Tunnel junction setpoint, 5 mV, 20 pA. All topographs have the same scale. (B) Pump-probe measurements on Fe_3 for each configuration in (A) as the nanomagnet stays in each Néel state. The pump-probe signal is normalized to 1 at zero delay time for clarity. Solid lines are exponential fits. (C) Spin relaxation time as a function of external magnetic field measured on Fe_3 when the nearby nanomagnet stays in different Néel states. The sensor-nanomagnet separation is 2.2 nm (shown in (A) third panel). Throughout the measurement, we use the same spin-polarized tip and tunnel junction setpoint, 5 mV, 200 pA. The error bar is comparable to the symbol size. Solid lines are linear fits. (D) Time traces of the pump-probe signal measured on Fe_3 with different pump voltages. The pump-probe signal is measured with 200 ns delay time and the sensor-nanomagnet separation is 2.2 nm.

Figure 3:

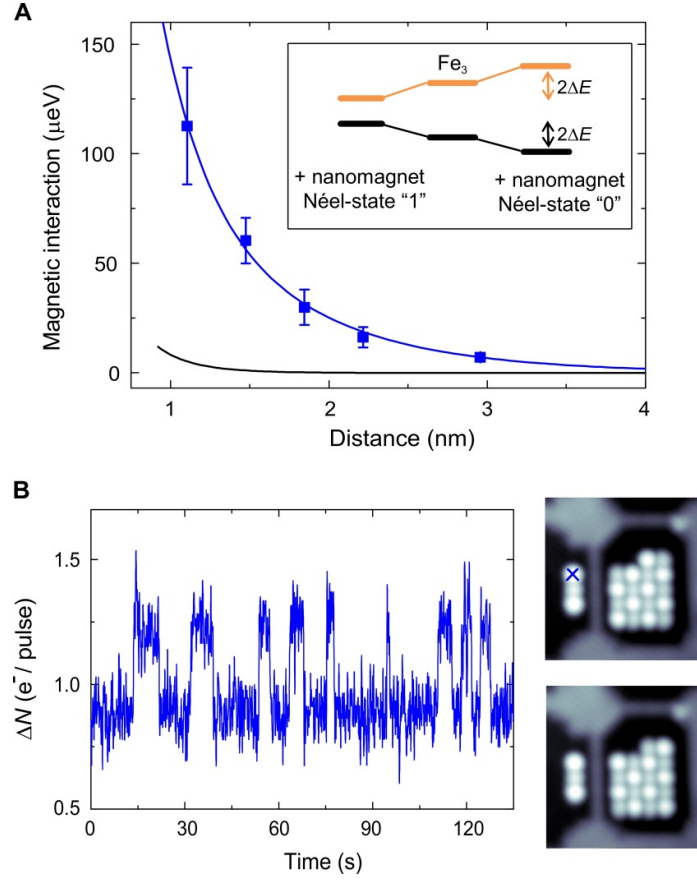


Fig. 3. Magnetic interaction between Fe_3 and nanomagnet. (A) Magnetic interaction energy, ΔE , between Fe_3 and nanomagnet for the configurations shown in Fig. 2A as a function of sensor-nanomagnet separation (blue points). The blue line is the calculated magnetic interaction between Fe_3 and nanomagnet with exponentially decaying exchange interaction between individual Fe atoms in them. The black line is the calculated magnetic dipolar interaction between Fe_3 and nanomagnet. Inset: energy diagram of the ground and first excited spin states of Fe_3 without and with the magnetic interaction with the nanomagnet. (B) Time trace of the pump-probe signal measured on Fe_3 resulting from Néel-state switching of a nanomagnet located on a different Cu_2N patch. Accompanying topographs show the sensor-nanomagnet configuration and position of the tip during pump-probe measurement (blue cross). Image size, $(7.7 \times 7.7) \text{ nm}^2$. Tunnel junction setpoint, 5 mV, 10 pA.

Figure 4:

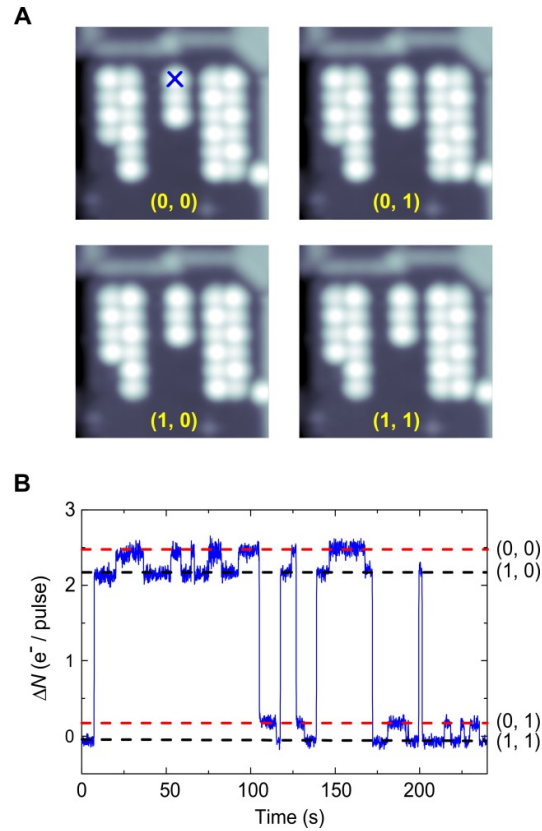


Fig. 4. Simultaneously sensing the spin states of two Fe nanomagnets. (A) STM constant current topographs showing four different states of the spin environments of Fe₃, labeled as (0, 1), (0, 1), (1, 0) and (1, 1). The first number indicates the magnetic state of the left nanomagnet and the second number refers to the state of the right nanomagnet. Image size, $(7.5 \times 7.5) \text{ nm}^2$, tunnel junction setpoint, 5 mV and 20 pA. (B) Time trace of the pump-probe signal measured on Fe₃ (tip position is marked by a blue cross in A). The delay time between pump and probe pulses is 180 ns. External magnetic field, 1.5 T, tunnel junction setpoint, 5 mV, 500 pA.

Supporting Material for

Non-locally sensing the spin states of individual atomic-scale nanomagnets

Shichao Yan*, Luigi Malavolti, Jacob A. J. Burgess, Sebastian Loth*

*Email: sebastian.loth@mpsd.mpg.de (S.L.); yansc@illinois.edu (S.Y.)

Materials and Methods

Sample preparation

All experiments were conducted using a low-temperature and ultrahigh-vacuum STM equipped with a 2 T vector magnetic field (Unisoku USM-1300 ^3He). For all the measurements the temperature was maintained at 0.5 K, and the external magnetic field was aligned to the easy magnetic axis of Fe atoms in the Fe_3 spin sensor. The easy axis was parallel to the direction of the two nitrogen atoms neighboring each Fe atom and the alignment accuracy of the magnetic field was $\pm 3^\circ$ accuracy (S1). PtIr tips were sputtered with Argon and flashed by e-beam bombardment for ten seconds prior to use. The Cu(100) crystal was cleaned by several Ar-sputtering and annealing (850 K) cycles. After the last sputtering and annealing cycle that creates a clean Cu(100) surface, the monatomic copper nitride, Cu_2N , layer was prepared by nitrogen sputtering at 1 kV and annealing to 600 K. Then, the sample was precooled to 4 K and Fe atoms were deposited onto the cold sample by positioning it in a low flux of Fe vapor from an Knudsen cell evaporator.

The Fe_3 quantum spin sensor was built by positioning Fe atoms 0.72 nm apart on the Cu binding sites of the Cu_2N surface by vertical STM atom manipulation technique (S2). The Fe_3 was built along the easy axis of Fe atoms in it. Fe_3 is a quantum magnet and the spin relaxation from the first excited spin state to the spin ground state is due to quantum tunneling (S3). The target nanomagnets were assembled from Fe atoms by the same technique. The even-numbered antiferromagnetically coupled nanomagnets consisted of twelve or more Fe atoms are classical antiferromagnets which have two stable Néel states (S4). The spin-polarized tips were prepared by picking up 3 – 4 Fe atoms to the apex of the tip which yielded spin polarization $\eta \approx 0.1\text{-}0.3$ (calibrated with 2 T external magnetic field).

All electronic pump-probe measurement

An all-electronic pump-probe method was used to measure the spin relaxation time of the Fe_3 (S3). A sequence of alternating pump and probe voltage pulses was created by a pulse pattern generator (Agilent 81110A) and sent to the sample using semi-rigid coaxial wires. The

pump pulses excite the Fe₃ by inelastic scattering of tunneling electrons. The probe pulses detect the spin state of the Fe₃ because the tunnel magneto-resistance differs when the Fe₃ is in the excited state versus the ground state. Tunnel current resulting from the probe pulses was measured by lock-in detection at 690.6 Hz.

For the measurements shown in Fig. 2B the probe pulses were modulated on and off. This method removes the tunnel current contribution of the pump pulses from the lock-in signal. For the measurements shown in Fig. 1B, C, Fig. 2D, Fig. 3B and Fig. 4B the time delay between pump and probe pulses was modulated. This method removes any tunnel current contributions that are not due to time-dependent dynamics and records background-free time traces of the pump-probe signal (S5, S6). The average dynamical evolution of the Fe₃ was measured by slowly varying the time delay between pump and probe pulses, Δt . For increasing delay time the probability of Fe₃ still being in the excited state decreases exponentially. The spin relaxation time, T_1 , was determined by fitting an exponential decay function to the delay-time dependent tunnel current $I(\Delta t)$.

Characterizing Fe₃ with external magnetic field

The Fe atoms in Fe₃ are antiferromagnetically coupled as evidenced by the topographic contrast when imaged with a spin-polarized STM tip. The individual Fe atoms are well-described as $S = 2$ spin systems. With the external magnetic field larger than 0.2 T, the energy splitting between the spin ground state and the first excited spin state of Fe₃ is dominated by the Zeeman energy. Hence, it increases linearly with magnetic field. When increasing the external magnetic field by 1 T, the energy splitting of the two spin states is increased by:

$$\Delta E_B = g\mu_B\Delta B_z \left(\sum_{i=A,B,C} S_{ie}^z - \sum_{i=A,B,C} S_{ig}^z \right) = 464 \mu\text{eV} \quad (\text{S1})$$

Where ΔE_B is the change in energy splitting, g is the Landé g -factor which is approximately 2 for Fe atoms on Cu₂N surface (S3, S7), and μ_B the Bohr magneton. ΔB_z is the change in the magnetic field strength along the easy-axis of the Fe atoms in Fe₃. S_{ie}^z and S_{ig}^z are the z -component of the spin operator of the i -th Fe atom for the first excited state and the ground state of Fe₃.

We measured the magnetic field dependence of T_1 to calibrate the linear coefficient α in Eq. (1) of the main text for each location in which the Fe₃ spin sensor was. We find that T_1 increases linearly with increasing magnetic field in every location because ΔE_B scales linear with magnetic field. The linear slope, however, varies between different locations.

Tuning the signal-to-noise by external magnetic field and interaction with magnetic tip

When the nearby nanomagnet changes between its two magnetic states, the Fe₃ spin sensor switches between two different spin relaxation time constants. For each distance between Fe₃ and nanomagnet the change in T_1 upon nanomagnet switching (ΔT_1) is constant. The signal-to-noise ratio in the non-local sensing measurement scales with $\Delta T_1 / T_1$ (Fig. S2 and Fig. S3), and can therefore be improved by decreasing T_1 with external magnetic field (Fig. S2 D and Fig. S3 D) or

by applying a local exchange bias field to a side atom with the magnetic tip (Fig. S2 C and Fig. S3 C) (S3). Fig. S2 and Fig. S3 show that, in order to clearly detect the difference between the two spin relaxation curves, $\Delta T_1 / T_1$ has to be tuned to be larger than 0.1.

Figure S1:

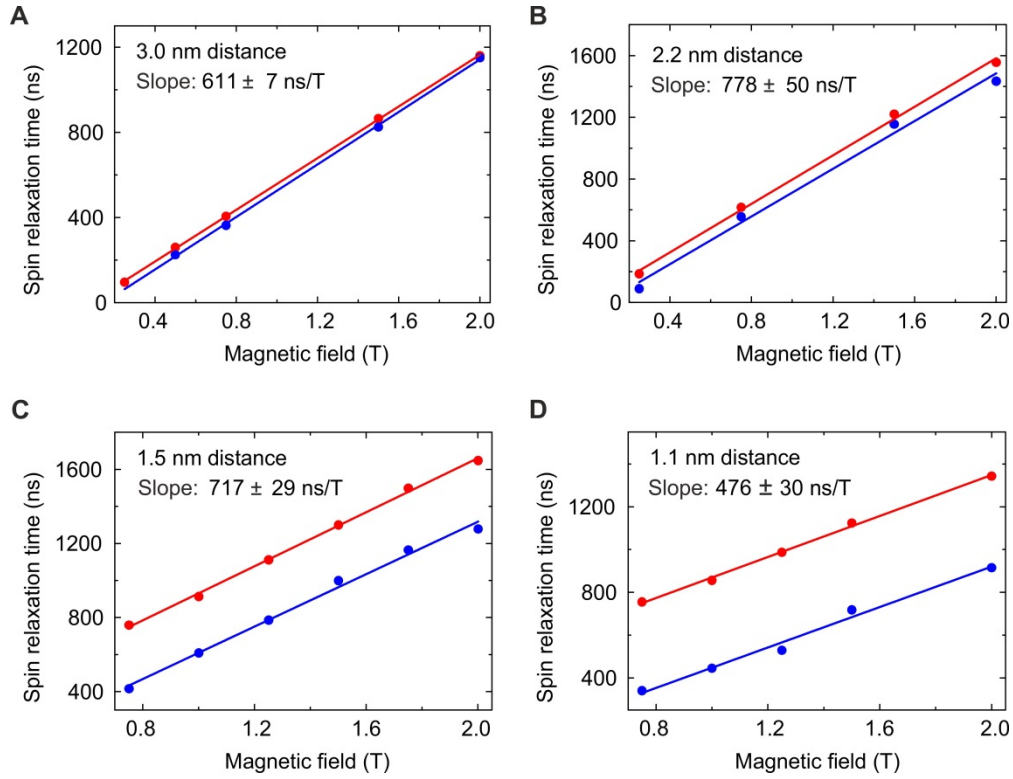


Fig. S1. Calibrating Fe_3 with external magnetic field. Spin relaxation time, T_1 , of Fe_3 as a function of external magnetic field. (A) for the configuration shown in Fig. 2A top panel with 3.0 nm separation between Fe_3 and nanomagnet. (B) for 2.2 nm separation as shown in Fig. 2A second panel. (C) for 1.5 nm separation as shown in Fig. 2A third panel. (D) for 3.0 nm separation as shown in Fig. 2A bottom panel. Red points are measured values of T_1 as the nanomagnet stays in Néel state "0" and blue points are measured for Néel state "1". Solid lines are linear fits and the fitted slope is indicated in each plot.

Figure S2:

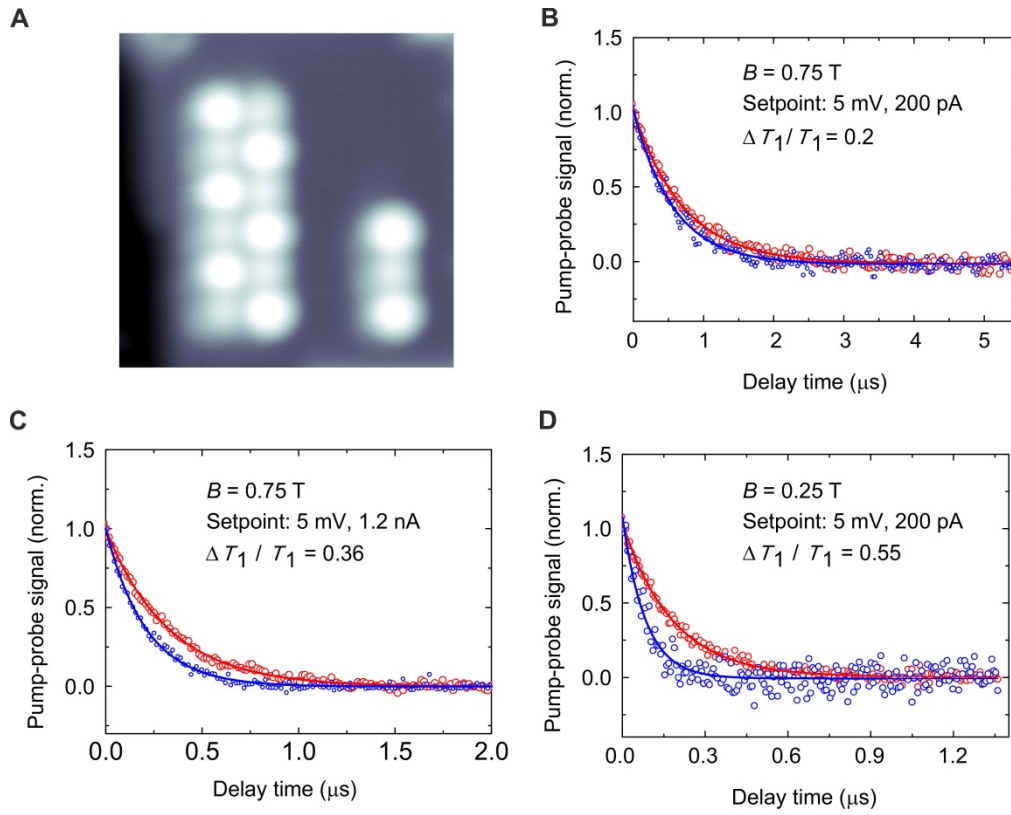


Fig. S2. Improving the signal-to-noise by external magnetic field or local magnetic field exerted by the magnetic STM tip. (A) Constant current topograph of a Fe₃ and a nanomagnet recorded with a spin-polarized tip. Image size, (5.8×5.8) nm². The separation between Fe₃ and nanomagnet is 2.2 nm. (B) Red and blue dots show pump-probe spectra measured on Fe₃ as the nanomagnet is in different Néel states. Solid lines are exponential fits. External magnetic field is 0.75 T external magnetic field and tunnel junction setpoint is 5 mV, 200 pA. (C) Same measurement as (B) but measured with 5 mV, 1.2 nA tunnel condition which will move the magnetic tip closer to Fe₃. The magnetic tip exerts a local exchange bias field on Fe₃ that acts analogous to a magnetic field and increases $\Delta T_1 / T_1$. (D) Same measurement as (B) but measured at 0.25 T external magnetic field. The difference between red and blue pump-probe curves in (C) and (D) is significantly more pronounced than in (B) because of an increased $\Delta T_1 / T_1$.

Figure S3:

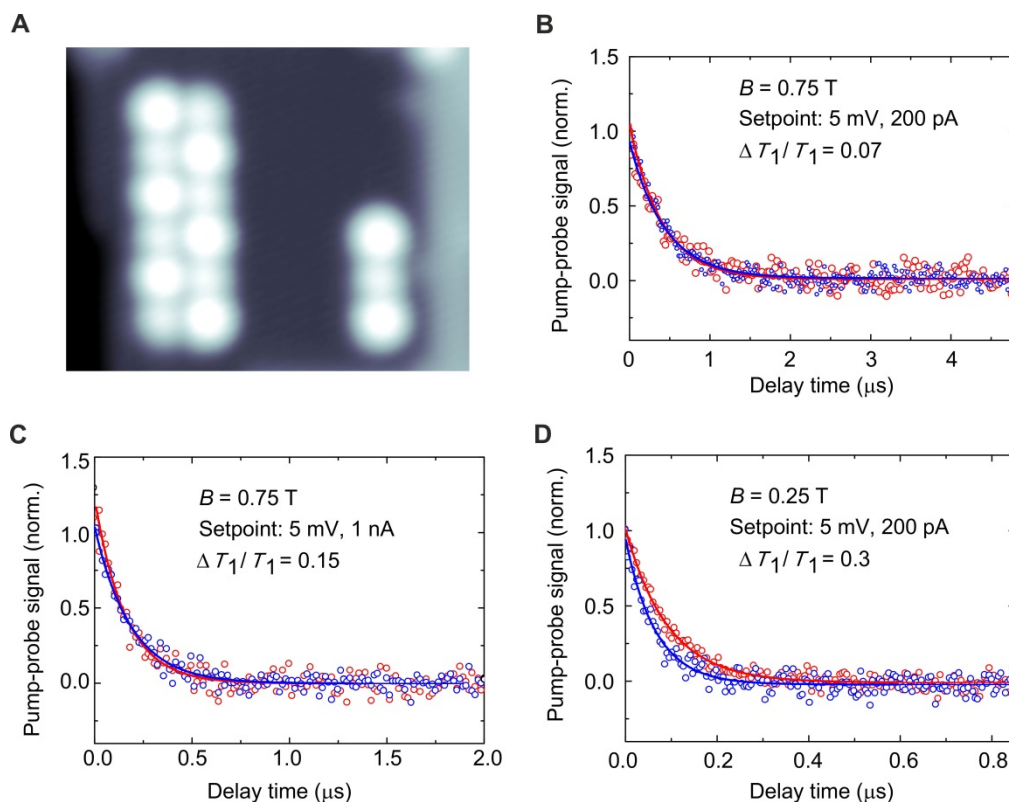


Fig. S3. Improving the signal-to-noise by external magnetic field or local magnetic field exerted by the magnetic STM tip. This figure shows the same measurements as shown in Fig. S2 but performed on the Fe₃ sensor for a separation of 3.0 nm between Fe₃ and nanomagnet.

Supplemental References:

- S1. S. Yan, D.-J. Choi, J. A. J. Burgess, S. Rolf-Pissarczyk, S. Loth *Nano Lett.* **15**, 1938 (2015).
- S2. L. Bartels, G. Meyer, K.-H. Rieder *Appl. Phys. Lett.* **71**, 213 (1997).
- S3. S. Yan, D.-J. Choi, J. A. J. Burgess, S. Rolf-Pissarczyk, S. Loth *Nat. Nano.* **10**, 40 (2015).
- S4. S. Loth, S. Baumann, C. P. Lutz, D. M. Eigler, A. J. Heinrich *Science* **335**, 196 (2012).
- S5. O. Takeuchi, R. Morita, M. Yamashita, H. Shigekawa *Jpn. J. Appl. Phys.* **41**, 4994 (2002).
- S6. I. G. Rau *et al.*, *Science* **344**, 988 (2014).
- S7. C. F. Hirjibehedin *et al.*, *Science* **317**, 1199 (2007).